# Spontaneous Curvatures of Copolymer Interfaces in Poor Solvents: Bilayer Morphology

**Anne L. Larsen and Eugene M. Terentjev***

*Cavendish Laboratory, University of Cambridge, J. J. Thomson Avenue, Cambridge, CB3 0HE, United Kingdom*

*Received June 23, 2006; Revised Manuscript Received October 4, 2006*

ABSTRACT: We compute phase diagrams for dilute AB diblock copolymers in poor solvent in the strong segregation limit (SSL), where we allow for vesicle morphologies with spontaneous curvature and finite radius. We compare monolayer and bilayer structures as well as the possibility of macroscopic phase separation. The phases are in general not thermodynamically stable with respect to macroscopic phase separation, but because of slow kinetics of transitions between states with close free energy, we can assume that the mono- and bilayer structures are sufficiently metastable. Thereby, we can justifiably map transitions between various phases with, e.g., bicontinuous and continuous structures in either solvent or copolymer. We show that the bilayer vesicles can be thermodynamically favorable compared to micellar structures for low volumetric asymmetry of the copolymer such that completely symmetric copolymers do not necessarily lead to lamellar structures or large vesicles without spontaneous curvature.

## 1. Introduction

The interplay between interfacial curvature and topology plays a central role in self-assembled soft materials, e.g., in cell membranes and in synthetic drug delivery systems. Amphiphilic block copolymers in water, like natural phosphor lipids, can self-assemble into various ordered mesophases.[1−3] For melts of diblock copolymers, it is well-known that there exists a variety of distinct phases, e.g., lamellar, cylindrical, and spherical morphology as well as the three-dimensional bicontinuous morphology,[5−7] which all have different interfacial curvatures. For diblock copolymers in solution, the picture gets more complex. Jain and Bates[8] have investigated the morphology of poly(1,2-butadiene-*b*-ethylene oxide) (PB-PEO) in water (1 wt %) as a function of molecular size and composition. They found four basic structural motifs: bilayers, Y-junctions, cylinders, and spheres. For a high degree of polymerization of the PB, a single-phase dispersion of branched wormlike micelles ($C_Y$) is followed by network formation in the regime of weight fractions where bilayers and cylindrical micelles are formed for low degrees of polymerization. This indicates a fundamental structural transition from classic two-component (surfactant/water) to three-component (surfactant/oil/water) phase behavior above a critical diblock copolymer molecular mass. These findings are consistent with the theoretical predictions recently developed[9−11] with traditional three-component (surfactant/oil/water) microemulsions. Döbereiner et al.[12,13] have also shown examples of phase diagrams with varying shapes of vesicles resembling the denoted $C_Y$ structure above.

At dilute concentrations of natural amphiphiles in water, bilayer structures with a thickness of only a few nanometers can form. Small amphiphiles of natural origin have inspired the engineering of higher molecular weight synthetic systems defined as superamphiphiles,[14] which include linear diblock copolymers. Discher et al.[15−17] have prepared polymersomes from such superamphiphiles and reported giant vesicles (20−50 $\mu$m) with layer thicknesses of up to 8 nm.

Development of the scaling concepts[18] and application of these ideas to micellization phenomena provided the power-law dependences for the equilibrium parameters of spherical aggregates. A number of experimental studies confirmed the general features of the theoretical predictions for properties of, e.g., spherical micelles. However, the experimentally measured values of the corresponding exponents often deviate from the theoretical predictions.[19] The discrepancies are usually attributed to slow kinetics and lack of system equilibration, sample impurities, and molecular weight polydispersity.

In early theoretical studies, the scaling model was used to delineate the scaling laws for parameters of equilibrium micelles.[20−24] This was done by balancing the two dominant contributions to the free energy of the micelle, i.e., the elastic energy of the corona and the surface energy of the core. The elastic energy of the core and all numerical coefficients were omitted.

A recent paper by Zhulina et al.[25] treats the boundaries between spheres, cylinders, and vesicles in copolymer micelles in detail as a function of the relevant variables. In addition to retaining all three contributions to the free energy (interfacial tension, corona crowding, and core stretching), numerical coefficients are evaluated. Of particular relevance is the finding that the free energies of the three traditional shapes (spherical, cylindrical, and lamellar) are very close in the regime of crew-cut micelles, which rationalizes the prevalence of coexisting spheres and cylinders and cylinders and vesicles. However, their model does not take into account the existence of small vesicles with curvature and thereby the different number of diblocks in the inner and outer layer. Additionally, they could not describe the bicontinuous network phase within the framework of their model. These details are taken into account in the present work by applying the results for polymer brushes[26−28] to calculate a lower bound on the free energy.

Another means of getting insight into the morphology of diblock copolymers is simulations, and there exists a variety of simulations based on a new Monte Carlo technique.[29,30,9] However, at the moment the simulations are limited to describing only certain chosen morphologies. An interesting example

* Corresponding author. E-mail: emt1000@cam.ac.uk.

10.1021/ma061417d CCC: $33.50 
Published on Web 12/05/2006

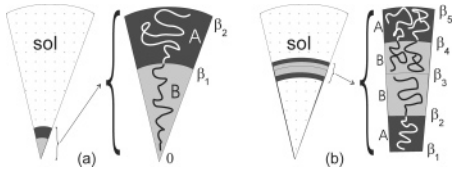


**Figure 1.** Illustration of the reference volume for (a) the micelle and (b) the vesicle. The micelle reference geometry contains one polymer only. The vesicle illustration shows $n = 2$ such that the reference volume contains three polymers and therefore allows for spontaneous curvature.

is the work of Tlusty et al.[30] who simulate the 3-fold "Y-like" junction in microemulsions and thereby accounts for the multiply connected sponge in which the water and oil domains are both continuous.

The present work is a natural extension of the preceding article,[31] where micellar morphologies are modeled and discussed. By micelle we mean a single-layer morphology where there is no solvent inclusion in the center of the geometry (i.e., a dense sphere or rod), and by vesicle we mean a double-layered morphology with solvent on both sides of the resulting membrane (i.e., a hollow shell), see Figure 1. Here we deal in detail with the spherical vesicle formation with its free energy expression derived in Section 2.1. In Sections 2.2−2.3, we apply the model to the tubular and bicontinuous vesicles. The bicontinuous vesicle can be shown to be a 3-D bicontinuous network. We furthermore apply the model to describe the multilayer, macroscopic phase separation in Section 2.4. We compare the spherical vesicle to the lamellar morphology, which by Zhulina et al.[25] was assumed to resemble a vesicle with infinite large curvature, and with macroscopic phase separation in Section 3.1. We proceed to discuss 3-D networks in Section 3.2. Finally, in Section 4, model predictions of phase diagrams including the micellar morphologies are combined with the vesicle structures are shown.

## 2. Theory

In the classical model of Olmsted and Milner,[32] the free energy is calculated per diblock chain. Therefore, the presence of solvent and the possibility of vesicular double layers with spontaneous curvature introduce the need for some modifications of the original model. The model presented here is a natural extension of the preceding paper,[31] which already deals with the additional solvent and furthermore introduces a measure of the spontaneous curvature. This extension allows us to determine the radius of the vesicle, in contrast to models which do not take into account curvature but assume that the lamellar morphology resembles the vesicular morphology if the vesicles are very large and thereby have negligible spontaneous curvature. Both diblock−diblock interaction and solvent−diblock interaction are assumed to be in the strong segregation limit (SSL), i.e., $\chi N \rightarrow \infty$ such that all interfaces are sharp. In the strong segregation limit, we can furthermore ignore the translational entropy of the junction points, which scales logarithmically with molecular weight and is thus subdominant.[32]

The model relies, as presented in ref 31, on the ratio of the cross-sectional area at a height $z$ relative to that of the outer surface, in an infinitesimal wedge of height $R$: $a(z/R) \equiv A(z)/A(R)$. It is important to emphasize that $R$ is not the absolute radius of the vesicle but is the radius of the reference geometry, which is changed with the amount of solvent due to the changed volume balance. However, the absolute value of the vesicle radius will not depend on the amount of solvent. The function $a(\beta)$ is equal to unity for the lamellae (L), $\beta$ for cylinders (C), $\beta(2-\beta)$ for the ordered bicontinuous double-diamond (B), and $\beta^2$ for spheres (S).[32] The same area functions can be applied directly to the vesicular structures.

The locations of the dividing surfaces are determined by setting the relative volume between the dividing surfaces equal to the volume fraction of the component between the two surfaces $\phi_i$:

$$v(\beta_x) - v(\beta_z) = \int_{\beta_z}^{\beta_x} \mathrm{d}y\, a(y) = \phi_i v(1) \tag{1}$$

where $\beta_x$ and $\beta_z$ are the outer and inner normalized distances, respectively, of the dividing surfaces measured from the center of the wedge, and $v(1)$ is the relative volume parameter derived from the area function $v(\beta) = \int_0^\beta \mathrm{d}y\, a(y)$.

For comparison with the micellar phases, the dividing surfaces for the micellar and vesicular morphologies are illustrated in Figure 1. For the morphologies with bilayers, the parametrization with two relative positions derived directly from the volume fractions, as shown for the micellar morphologies in the preceding work (Figure 1a) is insufficient. There are five relative positions describing each of the dividing surfaces (S−A, A−B, B−B, B−A, A−S), Figure 1b. The positions depend not only upon the position of the inner S−A interface ($\beta_1$), but also on the number of molecules in the outer layer $n$ compared to that of the inner layer, which is set equal to 1 for the reference volume such that each reference volume contains $n + 1$ molecules. $n \neq 1$ allows accounting for spontaneous curvature of the vesicle bilayer, and the area function gives the freedom to place the bilayer at an arbitrary position $\beta_1$ from the vesicle center.

The total volume balance has changed from the monolayer phases of ref 31 and now comprises the parameter $n$ as well as the volume fraction of polymer $\phi$:

$$(n+1)\Omega = A(R)Rv(1)\phi \tag{2}$$

where $\Omega = \Omega_A + \Omega_B$ is the absolute volume of the diblock polymer, that is, a sum of the partial volumes of the two species. By introducing the area function as defined earlier, the surface area of a given interface $i$ in an arbitrary morphology can be expressed as:

$$s_i = a(\beta_i)A(R) = \frac{a(\beta_i)(n+1)\Omega}{v(1)R\phi} \tag{3}$$

Equation 3 holds for all the morphologies (even monolayers, which are defined by $n = 0$) because the absolute volume of the core component is not derived from the surface area of the dividing surface but rather from an overall volume balance.

To obtain a phase diagram as a function of molecular size and composition, it is convenient to define two ratios. The compositional asymmetry ratio is defined as:

$$k_\phi = \frac{\phi_A}{\phi_B}, \qquad \phi_A + \phi_B = \phi \tag{4}$$

The surface tension ratio is defined as the relation of the surface tension between the A species and the solvent ($\gamma_{AS}$), and the surface tension between the two species in the polymer ($\gamma_{AB}$):

$$k_\gamma = \frac{\gamma_{AS}}{\gamma_{AB}}, \gamma_{AB} + \gamma_{AS} = \gamma \tag{5}$$

The second constraint in eq 5 is not necessary, but it is

convenient in order to get the same magnitude of free energies and thereby to facilitate comparison.

The end-to-end distances of the separate diblocks $r_A$ and $r_B$ can be expressed in terms of the total end-to-end distance of the entire diblock $r_o$ for different systems:

$$r_{A,B} = \frac{r_o}{1 + (k_\phi \epsilon_F)^{\pm 1/2}} \tag{6}$$

see eqs 10−13 in ref 31 for details. The Fredrickson's asymmetry parameter is given by:[33]

$$\epsilon_F = \frac{\Omega_B}{r_B^2}\frac{r_A^2}{\Omega_A} \tag{7}$$

**2.1. The Free Energy of the Spherical Vesicle.** In their attempt to include vesicles into their description, Zhulina et al.[25] consider what is essentially a bilayer in a flat lamellar conformation. This may well represent a very large vesicle where the curvature is negligible. We shall allow for the spontaneous curvature of the bilayer by introducing a parameter $n$, which accounts for imbalance of number of molecules between the inner and outer layers. Thereby, we include the possibility for the formation of small vesicles, where the bilayer thickness is not vanishing in comparison to the radius of the vesicle, and we can furthermore determine the equilibrium radius of the vesicle.

For our model, we need the positions of the dividing surfaces as a function of the number of diblocks in the outer layer ($n$) and the reference position of the innermost surface ($\beta_1$). The four other relative positions of the dividing surfaces can be written as a function of the position of the inner surface of the vesicle ($\beta_1$) and $n$ via the volume balance given in eq 1. A balance over the volume of the A species of the inner diblock, which is fraction $\phi_A/(1+n)$ of the total relative volume $v(1) = 1/3$, occupying the relative volume given by $[\beta_2^3 - \beta_1^3]/3$ gives:

$$\beta_2 = \left(\beta_1^3 + \frac{1}{n+1}\phi_A\right)^{1/3} \tag{8}$$

Similarly, the volume balances for the other layers in Figure 1b give:

$$\beta_3 = \left(\beta_1^3 + \frac{1}{n+1}\phi\right)^{1/3} \tag{9}$$

$$\beta_4 = \left(\beta_1^3 + \frac{1}{n+1}\phi + \frac{n}{n+1}\phi_B\right)^{1/3} \tag{10}$$

$$\beta_5 = (\beta_1^3 + \phi)^{1/3} \tag{11}$$

The relative positions of the dividing surfaces are no longer known a priori from volume balances because $n$ and $\beta_1$ can be chosen arbitrarily and are set to be the minimizing parameters for the free energy.

In contrast to previous work,[31] the reference wedge now contains $n+1$ polymers, and to keep the notation of free energy per one chain, we write the free energy expression as:

$$F_{ves} = \sum_{k=1}^{4} F_{int,k} + \sum_{j=1}^{2}\sum_{I=A,B} [n^{j-1} F_{strI,j}(n,\beta_1)] \tag{12}$$

where the first summation covers the four interfaces (excluding the "free" B−B interface) and the double summation covers the stretching of the two diblock species in each layer. The first term in eq 12, representing the sum of the interfacial energies per molecule, can be written as:[32]

$$F_{int} = \frac{1}{1+n}\frac{3\Omega}{\phi R}(\gamma_{AS}[\beta_1^2 + \beta_5^2] + \gamma_{AB}[\beta_2^2 + \beta_4^2]) \tag{13}$$

The stretching free energy per molecule, which is the full second term in eq 12, is given by:[32]

$$F_{str} = \frac{3\pi^2 R^2}{8\phi}\left(\frac{1}{\phi_A'^2}[I_A' + I_A''] + \frac{1}{\phi_B'^2}[I_B' + I_B'']\right) \tag{14}$$

where $\phi_A'$ and $\phi_B'$ are the volume fractions of A and B within the copolymer (i.e., $\phi_A' + \phi_B' = 1$). The stretching integrals for bilayer morphologies can be written as:

$$I_A' = \int_0^{b_2-\beta_1} dy\, a(\beta_2 - y)y^2 \tag{15}$$

$$I_A'' = \int_0^{\beta_5-\beta_4} dy\, a(\beta_4 + y)y^2 \tag{16}$$

$$I_B' = \int_0^{\beta_3-\beta_2} dy\, a(\beta_2 + y)y^2 \tag{17}$$

$$I_B'' = \int_0^{\beta_4-\beta_3} dy\, a(\beta_4 - y)y^2 \tag{18}$$

where $a(\beta_i \pm y) = (\beta_i \pm y)^2$ for the spherical vesicle. This can be derived directly from eq 19 in the preceding paper[31] with the new expression for the surface coverage (eq 2 here). The explicit evaluation of eq 14 is given in the Appendix. It is not completely obvious that the stretching free energy has no direct dependence on the number of molecules in the outer layer $n$, but the free energy does however depend indirectly on $n$ via the outer stretching integrals $I_A''$ and $I_B''$. The difference with the analogous geometric integrals in previous work for micellar morphologies is in the modified volume balances as well as the existence of both an inner and outer layer, where the stretching of the respective diblock species is not equal except in the case of an infinitely large vesicle, where the curvature is negligible. This would however exclude the spherical wedge from consideration because the vesicle would rather be approximated by the lamellar morphology.

Eqs 15−18 can be expressed in terms of $\beta_1$ and $n$, and then the minimized total free energy of the system per polymer molecule can be written as (see eq 26 of ref 31):

$$F(n,\beta_1,R) = K_{str}(n,\beta_1)R^2 + \frac{K_{int}(n,\beta_1)}{R} \tag{19}$$

Minimization of the free energy with respect to $R$ (analogous to the that of the micellar morphology in ref 31) gives:

$$F(n,\beta_1) = (2^{1/3} + 2^{-2/3})\cdot K_{str}(n,\beta_1)^{1/3}\cdot K_{int}(n,\beta_1)^{2/3} \tag{20}$$

where $K_{int}(n,\beta_1)$ and $K_{str}(n,\beta_1)$ are given by:

$$K_{int}(n,\beta_1) = \frac{1}{1+n}\frac{3\Omega}{\phi}(\gamma_{AS}[\beta_1^2 + \beta_5^2] + \gamma_{AB}[\beta_2^2 + \beta_4^2]) \tag{21}$$

$$K_{str}(n,\beta_1) = \frac{3\pi^2}{8\phi}\left(\frac{1}{\phi_A r_A^2}[I_A' + I_A''] + \frac{1}{\phi_B r_B^2}[I_B' + I_B'']\right) \tag{22}$$

Minimization of the above expression with respect to $n$ and $\beta_1$ gives the vesicle size ($\beta_1 R$) and the spontaneous curvature

($n$). We assume that the brush is not compressible in any layer. This is an approximation, but it is reasonable because compressional forces are of higher magnitude than stretching forces.[26] It is a necessary constraint because the model does not include compressional forces and $n \rightarrow \infty$ would minimize the free energy expression by compressing the inner layer, which will have vanishing stretching free energy but should have high compression energy. We must remind the reader that the overall volume of the system, and each of its components, is of course conserved; here, we are discussing the uniaxial compression of the layer along its normal. To ensure that there is no compression of the two polymer brushes in any of the layers, the thickness of each layer is compared to the equilibrium end-to-end distance of the relevant copolymer species. The four resulting constraints can be written:

$$(\beta_2 - \beta_1)R_{\min} \geq r_A \tag{23}$$

$$(\beta_3 - \beta_2)R_{\min} \geq r_B \tag{24}$$

$$(\beta_4 - \beta_3)R_{\min} \geq r_B \tag{25}$$

$$(\beta_5 - \beta_4)R_{\min} \geq r_A \tag{26}$$

where $R_{\min}$ is the value of the radius of the reference geometry $R$ that minimizes $F$ (eq 19). Hereby, we limit ourselves to physical solutions. Additionally, we have to check for solutions with $\beta_1 = 0$. This is a sensible physical solution corresponding to a bilayer micelle, but the result is not a vesicle because there is no solvent inclusion. Such a morphology will in general be the result of a high A−S interfacial energy (large $k_\gamma$) because going from $\beta_1 > 0$ to $\beta_1 = 0$ decreases the number of A−S interfaces from 2 to 1, and thereby the overall interfacial free energy is lowered.

To eliminate the effect of the values of the material specific parameters $\Omega$ , $\gamma_o$, and $r_o$ on the value of the free energy, it is convenient to normalize the free energy by the energy of the reference lamellar morphology ($\beta_1 = 0$, $n = 0$) for a completely symmetric copolymer ($k_\phi = 1$, $\epsilon_F = 1$, and $\phi = 1$) in a system where the surface tension of all interfaces are equal ($k_\gamma = 1$):

$$F_L = (2^{-1/3} + 2^{-4/3})\left(\frac{\pi\Omega\gamma_o}{r_o}\right)^{2/3} \tag{27}$$

For the derivation of the above equation, see the preceding paper.[31] Thereby, the normalized free energy for the spherical vesicle (and all other morphologies in general) can be written as:

$$F^*(n,\beta_1) = \frac{F(n,\beta_1,R)}{F_L} = K^*_{str}(n,\beta_1)^{1/3}\cdot K^*_{int}(n,\beta_1)^{2/3} \tag{28}$$

where the normalized constants can be expressed purely in terms of the two key parameters ($k_\gamma$ and $k_\phi$) and are for the spherical vesicle given by:

$$K^*_{int}(n,\beta_1) = \frac{1}{1+n}\frac{3}{\phi}\left(\frac{k_\gamma}{1+k_\gamma}[\beta_1^2 + \beta_5^2] + \frac{1}{1+k_\gamma}[\beta_2^2 + \beta_4^2]\right) \tag{29}$$

$$K^*_{str}(n,\beta_1) = \frac{3(1+k_\phi)}{2\phi}\left(\frac{(1+(k_\phi\epsilon_F)^{1/2})^2}{k_\phi}[I'_A + I''_A] + (1+(k_\phi\epsilon_F)^{-1/2})^2[I'_B + I''_B]\right) \tag{30}$$

**2.2. The Free Energy of Tubular Vesicles.** Following the same procedure as for the spherical vesicle case, we reach similar equations with only small modifications [$v(1)$ and $a(y)$ are changed]. The interfacial constant in the normalized free energy expression (eq 28) for the tubular vesicle ($v(1) = {}^1/_2$ and $a(y) = y$) can be written:

$$K^*_{int} = \frac{1}{1+n}\frac{2}{\phi}\left(\frac{k_\gamma}{1+k_\gamma}[\beta_1 + \beta_5] + \frac{1}{1+k_\gamma}[\beta_2 + \beta_4]\right) \tag{31}$$

with the relative positions of the interfaces given by:

$$\beta_2 = \left(\beta_1^2 + \frac{1}{n+1}\phi_A\right)^{1/2} \tag{32}$$

$$\beta_3 = \left(\beta_1^2 + \frac{1}{n+1}\phi\right)^{1/2} \tag{33}$$

$$\beta_4 = \left(\beta_1^2 + \frac{1}{n+1}\phi + \frac{n}{n+1}\phi_B\right)^{1/2} \tag{34}$$

$$\beta_5 = (\beta_1^2 + \phi)^{1/2} \tag{35}$$

The normalized stretching constant can be written as (refer to eq 62 in the Appendix for details):

$$K^*_{str}(n,\beta_1) = \frac{1+k_\phi}{\phi}\left(\frac{(1+(k_\phi\epsilon_F)^{1/2})^2}{k_\phi}[I'_A + I''_A] + (1+(k_\phi\epsilon_F)^{-1/2})^2[I'_B + I''_B]\right) \tag{36}$$

with the stretching integrals given by eqs 15−18 with $a(\beta_i \pm y) = \beta_i \pm y$.

**2.3. 3-D Networks.** In the preceding work,[31] the micellar phases were treated. The bicontinuous micellar structure was clearly a 3-D network, but the curved structure was a result of the assembly of the reference geometries. Spontaneous curvature as a result of different number of polymers in the inner and outer layer was therefore not accounted for. The bilayer network (denoted B), which is discussed in the preceding article, is generated from the assembly of the micellar reference geometries with "symmetric wedge" geometry. The resulting network is continuous in both solvent and polymer as discussed previously. The volume balances for the bicontinuous bilayer network (B) can be written:

$$\beta_1^2 - \frac{1}{3}\beta_1^3 = \frac{2}{3}\phi_B \tag{37}$$

$$\beta_2^2 - \frac{1}{3}\beta_2^3 = \frac{2}{3}\phi \tag{38}$$

Then the two relative positions can be found. The normalized free energy of the B morphology can then be calculated from eqs 33−35 in the preceding article,[31] with the integrals in the stretching free constant taking the form:

$$I_{B,B} = 3\int_0^{\beta_1} dy(\beta_1 - y)(2 - \beta_1 + y)y^2 \tag{39}$$

$$I_{A,B} = \int_0^{\beta_2-\beta_1} dy(\beta_1 + y)(2 - \beta_1 - y)y^2 \tag{40}$$

Another possibility for the polymers to form networks is the bilayer structure with spontaneous curvature (in the following denoted by $B_3$), i.e., a vesicular structure with $\beta_1 > 0$. This structure differs from the previous bilayer network structure by the spontaneous curvature and the fact that the structure has

two separate channels for solvent diffusion, inner and outer, compared to only one for the B structure.

For the bilayer network structure with spontaneous curvature ($B_3$), the four outer relative positions of the dividing surfaces can, as seen from the other vesicular morphologies, be written as:

$$\beta_2^2 - \beta_1^2 - \frac{1}{3}(\beta_2^3 - \beta_1^3) = \frac{2}{3}\frac{1}{n+1}\phi_A \tag{41}$$

$$\beta_3^2 - \beta_2^2 - \frac{1}{3}(\beta_3^3 - \beta_2^3) = \frac{2}{3}\frac{1}{n+1}\phi \tag{42}$$

$$\beta_4^2 - \beta_3^2 - \frac{1}{3}(\beta_4^3 - \beta_3^3) = \frac{2}{3}\left(\frac{1}{n+1}\phi_A + \phi_B\right) \tag{43}$$

$$\beta_5^2 - \beta_4^2 - \frac{1}{3}(\beta_5^3 - \beta_4^3) = \frac{2}{3}\phi \tag{44}$$

Following the same procedure as for the spherical vesicle case, we reach similar equations, again with only small modifications [$v(1)$ and $a(y)$ are changed]. The interfacial constant in the normalized free energy expression (eq 28) for the $B_3$ structure can be written as:

$$K^*_{int} = \frac{1}{1+n}\frac{3}{2\phi}\left(\frac{k_\gamma}{1+k_\gamma}[\beta_1(2-\beta_1)+\beta_5(2-\beta_5)] + \frac{1}{1+k_\gamma}[\beta_2(2-\beta_2)+\beta_4(2-\beta_4)]\right) \tag{45}$$

with the relative positions of the interfaces given by eqs 41−44.

The normalized stretching constant for the $B_3$ structure can be written as (refer to eq 62 in the Appendix for details):

$$K^*_{str}(n,\beta_1) = \frac{3(1+k_\phi)}{4\phi}\left(\frac{(1+(k_\phi\epsilon_F)^{1/2})^2}{k_\phi}[I'_A + I''_A] + (1+(k_\phi\epsilon_F)^{-1/2})^2[I'_B + I''_B]\right) \tag{46}$$

with the stretching integrals given by eqs 15−18 and the area functions defined by $a(\beta_i \pm y) = (y \pm \beta_i)(2 - y - \beta_i)$.

**2.4. Macroscopic Phase Separation.** Although we do not pursue the question of the stability of the various phases against macroscopic phase separation further, it is interesting to discuss the thermodynamical stability of the macroscopic phase separated situation as predicted by the model. In the cases where the minimization procedure for spherical and tubular vesicles yields $\beta_1 = 0$, the result can very likely be regarded as a macroscopic phase separation because each additional layer added in the geometry will minimize the free energy (at least for the lamellar case each additional layer will always minimize the free energy because the stretching free energy and interfacial area do not change from layer to layer). If we imagine a multilayered spherical vesicle with $q > 2$ layers with $n_i$, $i = 1{:}q$ copolymers per layer (with $n_1 = 1$), we can write the normalized interfacial free energy for the multilayer spherical vesicle (MSV) as:

$$K^*_{int,MSV}(n_i,\beta_1) = \frac{3}{\phi}\left(\frac{k_\gamma}{1+k_\gamma}[\beta_1^2 + \beta_{2q+1}^2] + \frac{1}{1+k_\gamma}\sum_{i=1}^{q}\beta_{2i}^2\right) \tag{47}$$

At macroscopic phase separation, $q \to \infty$, and therefore, $R_{min} \to \infty$, which leads to negligible curvature, i.e., lamellar morphology where $n_i = 1$ for all layers. This simplifies the picture such that the interfacial free energy of the MSV approaches that of the multilayer lamellar (ML) morphology with a normalized stretching free constant given by:

$$K^*_{int,ML} = \frac{1}{\phi}\left(2\frac{k_\gamma}{1+k_\gamma} + \frac{q}{1+k_\gamma}\right) \tag{48}$$

In a similar way, the stretching free energy expressions for the macroscopic phase separation consisting of $q$ lamellar bilayers can be written as:

$$K_{str,ML} = \frac{\pi^2}{8\phi}\left(\frac{1}{\phi_A t_A^2}\sum_{i=1}^{q} I_{A,i} + \frac{1}{\phi'^2_B}\sum_{i=1}^{q} I_{B,i}\right) \tag{49}$$

where $\sum I_A$ and $\sum I_B$ are sums of the stretching free integrals of the lamellar morphology, which via a volume balance over the $q$ bilayers can be shown to reduce to:

$$\sum_{i=1}^{q} I_A = \sum_{i=1}^{q}(\beta_{2i-1} - \beta_{2i-2})^3 = \sum_{i=1}^{q}\left(\frac{\phi'_A\phi}{q}\right)^3 = \frac{\phi_A^3}{q^2} \tag{50}$$

$$\sum_{i=1}^{q} I_B = \sum_{i=1}^{q}(\beta_{2i} - \beta_{2i-1})^3 = \sum_{i=1}^{q}\left(\frac{\phi'_B\phi}{q}\right)^3 = \frac{\phi_B^3}{q^2} \tag{51}$$

The normalized stretching constant then reduces to:

$$K^*_{str,ML} = \frac{1}{q^2}\frac{1}{\phi}\frac{(1+(k_\phi\epsilon_F)^{1/2})^2}{(1+k_\phi)^2}\frac{1+k_\phi\epsilon_F}{k_\phi\epsilon_F} \tag{52}$$

The free energy per polymer molecule in the limit of $q \to \infty$ multilayers can then be written as:

$$\lim_{q\to\infty} F^*_{ML} = \lim_{q\to\infty}[(K^*_{int,ML})^{2/3}(K^*_{str,ML})^{1/3}] = \frac{1}{\phi}\left[\frac{(1+(k_\phi\epsilon_F)^{1/2})^2}{(1+k_\phi)^2}\frac{1+k_\phi\epsilon_F}{k_\phi\epsilon_F}\right]^{1/3}\left[\frac{1}{1+k_\gamma}\right]^{2/3} \tag{53}$$

i.e., in the case of no asymmetry at all ($\epsilon_F = k_\phi = k_\gamma = 1$), we have $\lim_{q\to\infty} F^*_{ML} = 1/(2^{1/3}\phi) \simeq 0.8F_L(\phi)$.

From the above, it is clear that there is a strong tendency to have the macroscopic phase separation as a global equilibrium such that all other phases are in fact metastable. However, because the model eliminates mixing entropy effects ($S \sim \phi \log \phi$), the free energy of the macroscopic phase separation is in fact a lower bound and the other phases may be favored over the macroscopic phase separation because they do not have as large an entropic penalty. There is an understanding, quite general for classical colloids and emulsions, that their structural stability is a kinetic concept and not a thermodynamic one,[34] so the prediction of macroscopic phase separation in the diblock copolymer solution being the thermodynamically stable morphology for most systems may very well be correct even though experiments show mono- and bilayer phases to be stable.

## 3. Results and Discussion

**3.1. Spontaneous Curvature of Spherical Vesicles.** The free energy of the spherical vesicle depends on both the relative position of the inner layer ($\beta_1$) and the number of polymers in the outer layer ($n$). In Figure 2, the free energies of possible vesicles formed in a given system are shown. The minimized

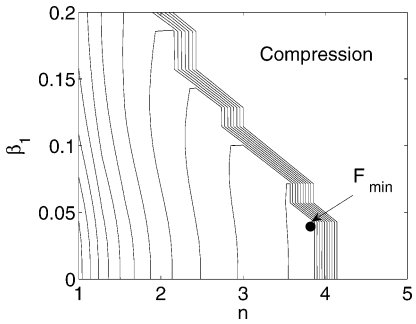


**Figure 2.** Contour map of the free energy for a given system ($k_\phi = 0.1$, $r_o/R^* = 0.01$, $k_\gamma = 1$) as function of the two minimizing parameters $n$ and $\beta_1$. The minimized free energy for the system ($F_{min}$) is marked with a ● and from the value of $\beta_1 = 0.043$, it is clear that the spherical vesicle is indeed a vesicle and not a bilayer micelle defined by $\beta_1 = 0$. For high values of $n$, most values lead to compression of the inner layer (solutions denoted by "compression").

free energy $F_{min}$ for the given system is indicated in the plot. It is clear from the figure that the number of polymers in the outer layer has a large influence on the free energy compared to that of the relative position, which does not influence the free energy to a large extent as long as it is below the compression threshold. For a given value of $\beta_1$, an increase in $n$ leads to a reduction in the free energy due to a reduction in interfacial free energy per molecule, but at a certain point (where the minimum value of the free energy is obtained), the increase in stretching free energies exceeds the reduction in interfacial free energy, and a small change in the value of $n$ leads to large increase in the free energy due to high stretching of the polymers in the outer layer before the inner layer is finally getting compressed.

In Figure 3, model predictions of different characteristics of the "minimized free energy" spherical vesicle are shown for different values of the volumetric asymmetry for a given value of the interfacial ratio $k_\gamma = 1$. The absolute radius ($R/R^*$) of the reference geometry goes through a minimum with increasing values of $k_\phi$ (see plot a). The value of the minimal radius depends on the ratio of interfacial free energy to stretching free energy, see eq 29 in preceding paper.[31] At this minimal radius, the number of polymers in the outer layer $n$ is at its highest (plot b), i.e., the reference geometry is quite broad, and the free energy is at its lowest (plot c), so it is clear that at this asymmetry, the polymers fit perfectly into the spherical vesicular geometry and thereby causing a very low extent of stretching. The absolute position of the inner and outer surface ($\beta_1 R/R^*$ and $\beta_5 R/R^*$) follows a similar pattern with a minimum at a given value of $k_\phi$ (see plot d). It is, however, clear that there is not a large difference of the membrane thickness ($\Delta\beta R/R^* = (\beta_5 - \beta_1)R/R^*$) with changing volumetric asymmetry. This agrees very well with the experimental evidence of similar thicknesses of all natural membranes arising from polymers with similar molecular weights but with different ratios between the two parts.[35]

In Figure 4, we illustrate how the reference geometry and the bilayer structure changes when the asymmetry parameter $k_\phi$ is increased. Because of the "geometric reversion" around the interface defined by $\beta_3$ of the polymers in the two layers of the bilayer morphology, very asymmetric polymers are not favorable in the vesicular phases and the free energy of the systems will resemble that of the lamellar morphology because the part of the reference geometry containing the polymers in most cases tends to become relatively square (as demonstrated in the figure) and get a small spontaneous curvature as the volumetric asymmetry is increased.

Systems where the interfacial energies dominate have a large tendency to aggregate into large humps of polymer, i.e., they tend to phase separate on a macroscopic scale. The results of macroscopic phase separation are discussed in more detail in Section 2.4. When the stretching free energies of the polymer are large, the cost of the additional interfaces from micellar morphologies to vesicular morphologies may be vanishing compared to the reduction obtained in stretching free energies. The model of Zhulina et al.[25] treats the lamellar morphology as

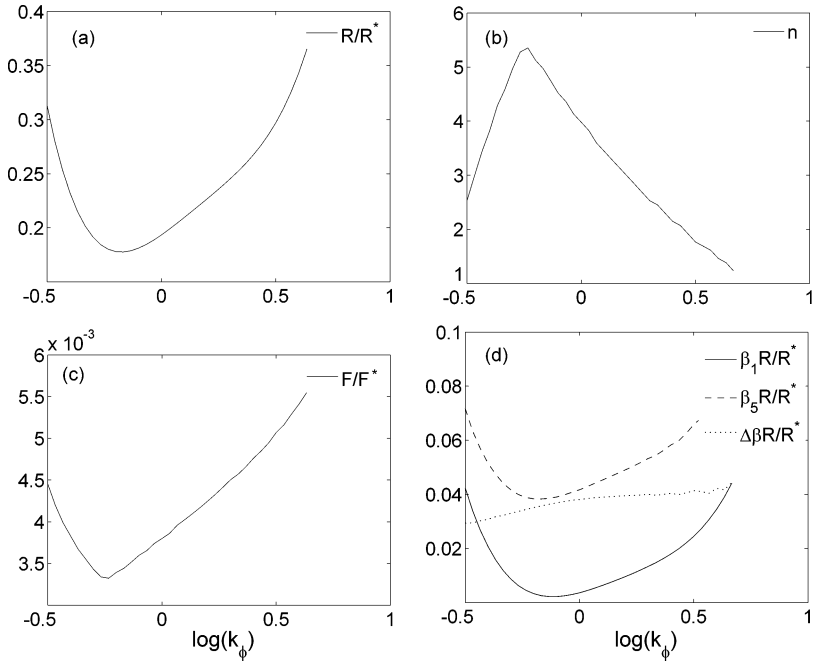


**Figure 3.** Different characteristics for the spherical vesicle morphology as function of the volumetric asymmetry: (a) The normalized radius of the reference geometry. (b) The number of polymers in the outer layer. (c) The normalized free energy of the minimized vesicle. (d) The normalized positions if the inner ($\beta_1 R/R^*$) and outer ($\beta_5 R/R^*$) surface of the vesicle as well as the bilayer thickness ($\Delta\beta R/R^*$). The range of values of $k_\phi$ are chosen such that systems where there are compression of either layers are omitted (i.e., $\log(k_\phi) < -0.5$ and $\log(k_\phi) > 0.67$ result in solutions where one or more layers are compressed). $r_o/R^* = 0.01$, $k_\gamma = \epsilon_F = \gamma = \Omega = 1$.

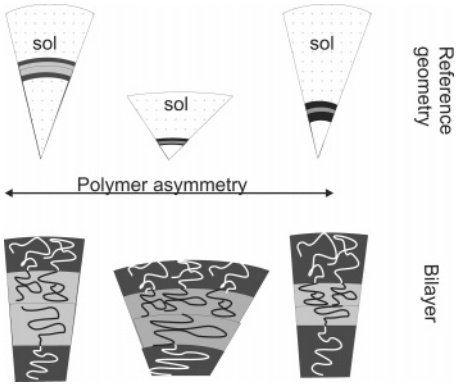


**Figure 4.** Illustration of how the reference geometry and the bilayer structure change with increasing values of the asymmetry parameter $k_\phi$. The wedges are widened for visual effect.

a vesicle with infinite curvature. Our model refines this assumption by (although limited to the strong segregation limit) calculating the free energy of morphologies with spontaneous curvature. In Figure 5, we have compared the free energy of three morphologies that are likely to dominate when the polymer asymmetry is small, namely the lamellar morphology (representing a vesicle with infinite curvature and no spontaneous curvature), the multilayer lamellar macroscopic phase separation (discussed in Section 2.4), and the spherical vesicle. The lamellar macroscopic phase separated morphology is included to keep in mind that the mono- and bilayer morphologies are never really thermodynamically stable compared to macroscopic phase separation. Of course, from Figure 5a, one may be lead to believe that the spherical vesicle is actually thermodynamically stable, but one can easily imagine that adding another bilayer (with $n_2$ and $n_3$ polymers) outside the first bilayer (with 1 and $n$ polymers) would decrease the free energy per polymer molecule even more, so the result would be macroscopic phase separation into a spherical "lump".

For diblock copolymers with small volumetric asymmetry, morphologies with relatively low curvature are preferred, i.e., lamellar or vesicular structures. In Figure 6, phase diagrams in which the lamellar (L), the multilayer lamellar (ML), and the spherical vesicle ($V_S$) are accounted for, are shown for four different values of the Fredrickson's asymmetry parameter $\epsilon_F$. In the plots, it is furthermore illustrated where the spherical vesicle is actually a spherical micellar bilayer structure (denoted by MV in the diagrams), which arises when $\beta_1 = 0$. The stability of the spherical vesicle is as expected highest when $k_\gamma < 1$ (i.e., the AB has stronger interfacial tension than the AS interface) because the transition of lamellar to the spherical vesicle morphology results in an increase in the outer AS surface, whereas the AB surface area per molecule may only be slightly influenced by the transition. It is obvious from the figure that

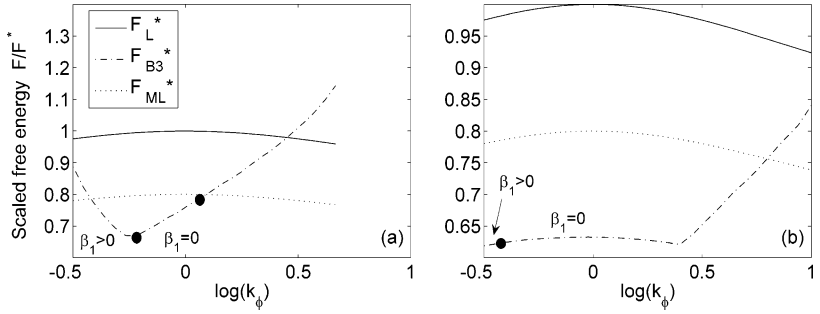


**Figure 5.** Comparison of the free energy of the lamellar, the multilayer lamellar (ML), and the spherical vesicle with spontaneous curvature for two different values of $r_o/R^*$. (a) $r_o/R^* = 0.01$, (b) $r_o/R^* = 0.001$. The ● illustrates the transition between a true vesicle with $\beta_1 > 0$ and a vesicle formed in the center of the reference geometry, i.e., a double-layer spherical micelle. $\epsilon_F = k_\phi = \gamma_o = 1$ and $\phi = 0.01$.

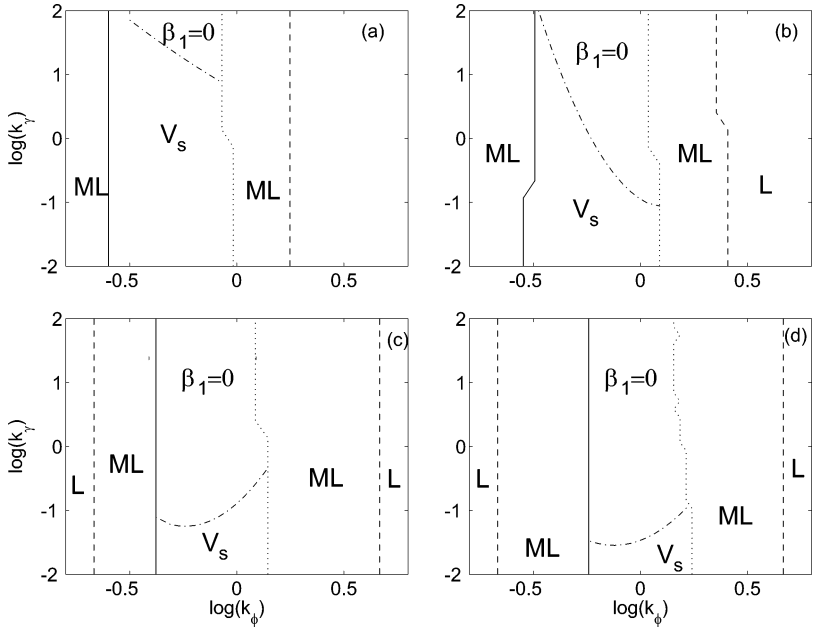


**Figure 6.** Phase diagrams for four different values of the Fredrickson's asymmetry parameter $\epsilon_F$ with increasing relatively rigidity of the A component. (a) $\epsilon_F = 0.5$, (b) $\epsilon_F = 0.75$, (c) $\epsilon_F = 1$, and (d) $\epsilon_F = 1.5$. The area marked with $\beta_1 = 0$ is double-layer spherical micelle. $r_o/R^* = \phi = 0.01$, $\gamma_o = \Omega = k_\gamma = 1$.

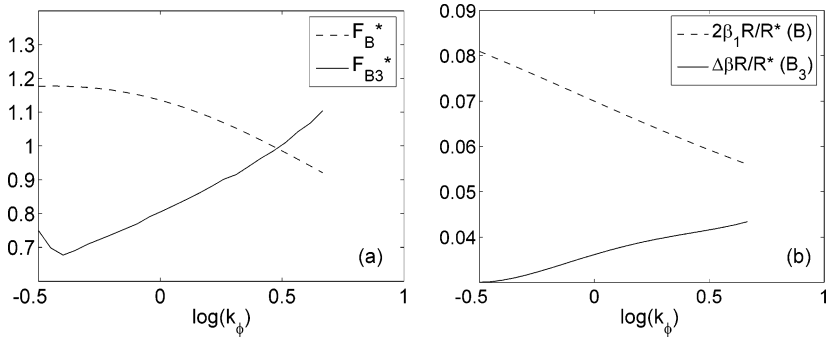


**Figure 7.** Comparison of (a) the normalized free energy and (b) the bilayer thickness in the two 3-D networks (B and $B_3$). $\phi = r_o/R^* = 0.01$, $k_\gamma = 0.1$, and $\epsilon_F = \Omega = \gamma_o = 1$.

the multilayer lamellar structure dominates, but it can be seen that with increasingly asymmetric polymers with a relatively rigid component B ($\epsilon_F < 1$) that the stability of the spherical vesicle increases. This can be explained by the structures with a rigid component B fitting more naturally into the outer layer such that it is only the A component in the inner layer that needs to be additionally stretched to fit into the reference geometry.

From the simplified phase diagram in Figure 6, it is clear that the assumption of Zhulina et al. in the weak segregation limit that the vesicle can be represented by the simpler lamellar morphology cannot be applied without loosing important structural properties of the vesicular structures in the strong segregation limit. However, it is clear that as the free energy of the vesicle approaches that of the lamellar phase, $R \rightarrow \infty$ and $n \rightarrow 1$ (illustrated in parts a and c of Figure 3, respectively, where the transitions $L \rightarrow V_S$ and $V_S \rightarrow L$ from Figure 6c is determined to occur for $\log(k_\phi) \simeq -0.6$ and $\log(k_\phi) \simeq 0.6$, respectively), which gives a clear indication of the close resemblance of two structures under certain circumstances. It is obvious that the spontaneous curvature minimizes the free energy compared to that of the lamellar morphology in certain situations, and thereby the spherical vesicle differs from the lamellar "vesicle" with infinite curvature.

**3.2. 3-D Networks.** The 3-D networks arising in diblock copolymer melts have been experimentally verified to be an "ordered bicontinuous double-diamond" phase.[36,37] The network phases in diblock copolymer solutions have far less homogeneity[6] and seem to be a mixture of coexisting phases. Within the framework of the model and the four defined area functions, it is possible to describe two network phases, namely the micellar and the vesicular bicontinuous structures. The two structures will be quite different because the micellar (B) structure is symmetric around the assembly axis and thereby have a rotation axis situated in the middle of the bilayer, i.e., at $\beta = 0$. The vesicular network has its rotation axis placed at the assembly axis as well, but the bilayer is situated away from this axis and there is no symmetry of the two layers around the interface of the two layers (i.e., at $\beta_3$) even in the case of no spontaneous curvature (i.e., $n = 1$). The layer thickness of the micellar structure will in general be larger than that of the vesicular structure because the micellar structure will have large stretching of the B component, which is restricted to center, and thereby the very narrow part of the "symmetric wedge" reference geometry. Because of these differences, both the free energy and the bilayer thickness vary from phase to phase, and from Figure 7, it is clear that the differences are rather large. The $B_3$ structure is stable with respect to the B structure at low asymmetries, which is rather intuitive because the micellar structure will be favored when the B component fits naturally into the narrow part of the center of the reference geometry, i.e., at high asymmetries: $\log(k_\phi) > 0$.

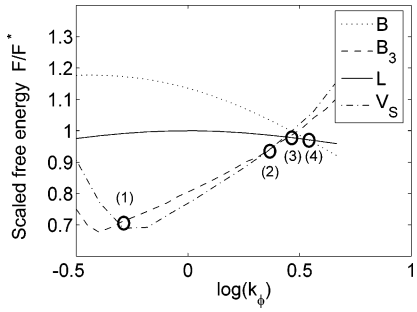


**Figure 8.** Illustration of the transitions between the four dominant phases at small volumetric asymmetry and low AS surface tension $k_\gamma = 0.1$. The transitions are: (1) $B_3 \rightarrow V_S$, (2) $V_S \rightarrow VB_3$, (3) $B_3 \rightarrow VL$, and (4) $L \rightarrow VB$. $\phi = r_o/R^* = 0.01$, and $\epsilon_F = \Omega = \gamma_o = 1$.

The normalized free energies of the four dominant phases at low volumetric asymmetry ($B_3$, B, L, and $V_S$) are compared in Figure 8. The phase transitions are also indicated in the plot, and it is clear that the free energy changes rather drastically around, e.g., the $B_3 \rightarrow V_S$ and $B_3 \rightarrow L$ transitions, whereas the free energy of, e.g., the $V_S$ and the $B_3$ phases are comparable in a large range of values of $k_\phi$ around the $V_S \rightarrow B_3$ transition. For copolymer solutions, a trend in available experimental data is the coexistence of many phases in what seems to be thermodynamically stable systems. The coexistence of, e.g., S and C and $V_C$ and $V_S$, is the rule rather than the exception.[6,7] Thereby the structural homogeneity of the phases is destroyed. From the free energy expression derived in this work, it can also be shown that the difference between the free energies of the $B_3$ and $V_C$ phases is vanishing for all possible systems. For the micellar structures discussed in the preceding work, the difference between the free energies of the bicontinuous B and the cylindrical C structures was limited as well, but because of the "geometric reversion" of the layers in the vesicular phases, the difference between these two phases (constructed from very similar reference geometries) gets even smaller. In the following, we will denote this complex phase resulting from a combination of vesicular cylinders and 3-D network as the $B_3$ phase even though the very ordered structure has been shown to be destroyed. Instead of imagining the $B_3$ morphology as a structure with constant curvature in two dimensions, it can easily be imagined as a phase with varying local curvature as one moves from a tubular vesicle regime to an "ordered bicontinuous double-diamond" regime.

## 4. Phase Diagrams

The "full" morphology diagrams are constructed from the free energy expressions given in this and the preceding paper

**Table 1. Different Structures Compared in the Morphology Diagrams**

| | continuous in | structure of polymer |
|---|---|---|
| L | | lamellar |
| $V_T$ | | tubular vesicle |
| $V_S$ | | spherical vesicle |
| B | polymer, solvent | bicontinuous network |
| $B_3$ | polymer, solvent (2) | tricontinuous network |
| C | solvent | cylindrical micelle |
| S | solvent | spherical micelle |
| ML | | macroscopic lamellar phase separation |
| MV | | macroscopic vesicle phase separation |

for the vesicular and micellar, respectively, morphologies. In Table 1, the different structures and their characteristics are summarized.

When determining the morphology diagram from the model, it is important to take into account all possible morphologies in order not to find a "false" minimum free energy morphology. Furthermore, it is, as discussed earlier, important to check if the vesicle formed is actually a double-layered micelle (i.e., $\beta_1$ of the respective morphology is equal to zero) because that indicates that all the copolymer will precipitate as one big mass of copolymer in alternating layers.

In Figures 9−11, phase diagrams are shown for three different values of the Fredrickson asymmetry parameter $\epsilon_F$ (refer to eq 7 for definition). The reversed structures discussed in Section 2.5 in the preceding article[31] are omitted due to the slight difference in calculating the lower bound of the free energy. As $\epsilon_F$ is increased (i.e., component A is getting more rodlike), the occurrence of the spherical micelle is decreased due to unfavorable curvature, as discussed in the preceding article. The same tendency is seen for the spherical vesicle but not to the same extent because the curvature is not as unfavorable as for the spherical micelle due to the occurrence of spontaneous curvature (i.e., $n$ can be increased to reduce the interfacial area per polymer molecule).

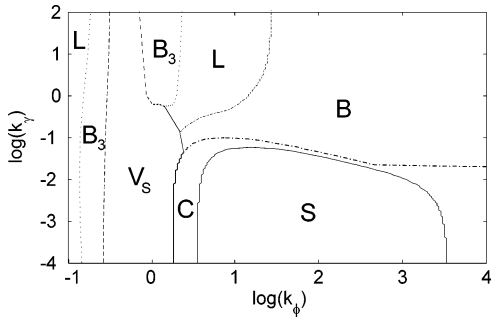


**Figure 9.** Phase diagram for a copolymer with a relatively rigid component B ($\epsilon_F = 0.5$). The $B_3$ phase is actually a phase consisting of both tubular vesicles and the tricontinuous bilayer network. $\phi = r_o/R^* = 0.01$, and $\Omega = \gamma_o = 1$.

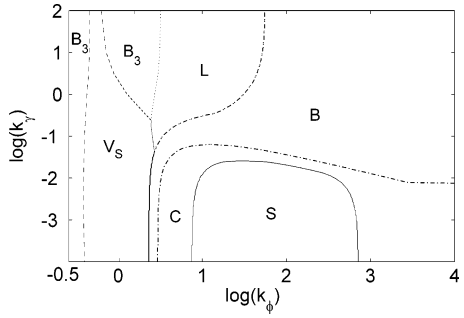


**Figure 10.** Phase diagram for a copolymer with no difference in rigidity of the two components ($\epsilon_F = 1$). The $B_3$ phase is actually a phase consisting of both tubular vesicles and the tricontinuous bilayer network. $\phi = r_o/R^* = 0.01$, and $\Omega = \gamma_o = \epsilon_F = 1$.

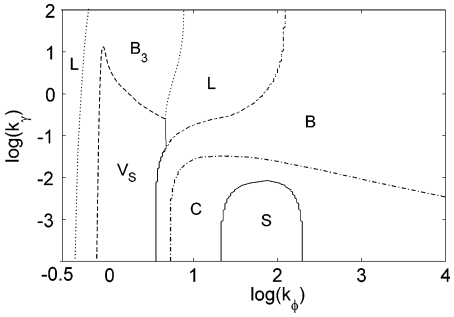


**Figure 11.** Phase diagram for a copolymer with a relatively rigid component A ($\epsilon_F = 2$). The $B_3$ phase is actually a phase consisting of both tubular vesicles and the tricontinuous bilayer network. $\phi = r_o/R^* = 0.01$, and $\Omega = \gamma_o = 1$.

## 5. Conclusion

In this study, we have developed a theory that describes the assembly of diblock copolymers into vesicular structures when dispersed in dilute and mutually poor solvent in the strong segregation limit. The solvent is assumed to be selective such that only component A and solvent interactions are allowed, in other words, the B− S interface tension is much higher than that of the A−S interface. We have extended the model to contain a measure $n$ of the spontaneous curvature, i.e., the number of polymers in the outer layer compared to that of the inner layer such that we can show that the addition of an additional interface, when going from the micellar to the vesicular morphology, can be energetically favorable.

We have compared the free energies of three vesicular structures ($B_3$, $V_T$, and $V_S$) with those of the micellar structures (L, C, B, and S) discussed in the preceding article and mapped their ranges of thermodynamic stability. The morphologies represent three solvent continuous structures (L, C, and B) and one bicontinuous structure (B) as well as one tricontinuous structure ($B_3$) with two distinctly different solvent channels.

We include a compressional constraint into the traditional melt model of Olmsted and Milner such that mathematical solutions arising from the minimization procedure over the two minimization parameters (the relative position of the inner surface of the vesicle and the number of polymers in the outer layer) do not lead to situations where either of the two brushes is compressed.

The vesicular morphologies occur as stable phases for diblock copolymers with small volumetric asymmetry ($k_\phi \simeq 1$). In most situations, the spherical vesicle is, however, not thermodynamically stable with regard to multilayer structures and thereby to macroscopic phase separation, but because of very slow kinetics, the spherical vesicle may seem thermodynamically stable.

The two network structures (B and $B_3$) have fairly different structural properties because the $B_3$ structure actually has two solvent channels compared to the B structure, which has only one kind of channel. It was found that it was hard to distinguish between the free energies of the tubular vesicle ($V_T$) and the 3-D network with spontaneous curvature ($B_3$), and it was argued that this result would indicate microscopic inhomogeneity of the resulting network phase with slightly varying curvatures depending on the local structure of the polymer.

Another important feature of the model is that it can effectively account for dilution effects. If the vesicles are formed in a dilute solution and further diluted afterward, the model

predicts that only the wedge radius $R$ and the relative positions of the interfaces $\beta_i$ change but in a way such that $R\beta_i$ is constant, which means that the absolute dimensions of the vesicle is conserved.

**Acknowledgment.** This research has been made possible by grants from Carlsbergfondet and EPSRC TCM/C3 Portfolio.

## Appendix

From eq 19 in the preceding paper,[31] we have following expression for the stretching free energy of the spherical geometry:

$$F_{str} = \frac{1}{\sigma}\frac{3\pi^2}{8}\int_0^{\sigma} d\sigma' \left[\frac{1}{r_A{}^2}h_A{}^2(\sigma') + \frac{1}{r_B{}^2}h_B{}^2(\sigma')\right] \quad (54)$$

This equation is valid for a reference geometry containing one copolymer chain, i.e., the free energy is calculated per molecule. We now have two layers, each resulting in two contributions to the stretching free energy. With one copolymer in the inner layer and $n$ copolymers in the outer layer, we can write the stretching free energy per polymer as function of the surface coverage:

$$F_{str} = \frac{1}{1+n}\frac{3\pi^2}{8}\left(\frac{1}{\sigma_{in}}\int_0^{\sigma_{in}} d\sigma'_{in}\left[\frac{1}{r_A{}^2}h_A{}^2(\sigma'_{in}) + \frac{1}{r_B{}^2}h_B{}^2(\sigma'_{in})\right] + \frac{n}{\sigma_{out}}\int_0^{\sigma_{out}} d\sigma'_{out}\left[\frac{1}{r_A{}^2}h_A{}^2(\sigma'_{out}) + \frac{1}{r_B{}^2}h_B{}^2(\sigma'_{out})\right]\right) \quad (55)$$

From volume balances at the two surfaces defined by $\beta_2$ and $\beta_4$, we can express the surface coverage of the inner and outer layer as:

$$\sigma_{in} = \frac{1}{1+n}\frac{\phi v(1)R}{\Omega a(\beta_2)} \quad (56)$$

$$\sigma_{out} = \frac{n}{1+n}\frac{\phi v(1)R}{\Omega a(\beta_4)} \quad (57)$$

The heights of the growing layers can be found from a volume balance over the reference geometry (refer to eqs 16 and 17 in ref 31):

$$v(\beta_2) - v(\beta_2 - h_A/R) = \sigma_{in}(h_A)\Omega_A a(\beta_2)/R \quad (58)$$

$$v(\beta_2 + h_B/R) - v(\beta_2) = \sigma_{in}(h_B)\Omega_B a(\beta_2)/R \quad (59)$$

$$v(\beta_4) - v(\beta_4 - h_B/R) = \sigma_{out}(h_B)\Omega_B a(\beta_4)/R \quad (60)$$

$$v(\beta_4 + h_A/R) - v(\beta_4) = \sigma_{out}(h_A)\Omega_A a(\beta_4)/R \quad (61)$$

From eqs 49−54, the change in surface coverage can be expressed in terms of the growing layer heights:

$$d\sigma_{in} = \frac{dh_A}{\Omega\phi'_A}\frac{a(\beta_2 - h_A/R)}{a(\beta_2)} \quad (62)$$

$$d\sigma_{in} = \frac{dh_B}{\Omega\phi'_B}\frac{a(\beta_2 + h_B/R)}{a(\beta_2)} \quad (63)$$

$$d\sigma_{out} = \frac{dh_B}{\Omega\phi'_B}\frac{a(\beta_4 - h_B/R)}{a(\beta_4)} \quad (64)$$

$$d\sigma_{out} = \frac{dh_A}{\Omega\phi'_A}\frac{a(\beta_4 + h_A/R)}{a(\beta_4)} \quad (65)$$

where $\phi'_A = \phi_A/\phi$ and $\phi'_B = \phi_B/\phi$. We can thereby solve the integrals in eq 47 by substitution of $d\sigma_j$, $j = in,out$ with $dh_i$, $i = A,B$, which then gives:

$$F_{str} = \frac{1}{1+n}\frac{3\pi^2}{8\Omega}\left(\frac{1}{\sigma_{in}a(\beta_2)}\left[\frac{1}{\phi'_A r_A{}^2}\int_0^{h^*_A} dh'_A h_A{}^2 a(\beta_2 - h_A/R) + \frac{1}{\phi'_B r_B{}^2}\int_0^{h^*_B} dh'_B{}^2 a(\beta_2 + h_B/R)\right] + \frac{n}{\sigma_{out}a(\beta_4)}\left[\frac{1}{\phi'_A r_A{}^2}\int_0^{h^{**}_A} dh'_A h_A{}^2 a(\beta_4 + h_A/R) + \frac{1}{\phi'_B r_B{}^2}\int_0^{h^{**}_B} dh'_B h_B{}^2 a(\beta_4 - h_B/R)\right]\right) \quad (66)$$

where $h^*_A = (\beta_2 - \beta_1)R$, $h^*_B = (\beta_3 - \beta_2)R$, $h^{**}_A = (\beta_5 - \beta_4)R$, and $h^{**}_B = (\beta_4 - \beta_3)R$. Substitution of $y = h_A/R = h_B/R$, finally gives:

$$F_{str} = \frac{1}{1+n}\frac{3\pi^2R^3}{8\Omega}\left(\frac{1}{\sigma_{in}a(\beta_2)}\left[\frac{1}{\phi'_A r_A{}^2}\int_0^{\beta_2-\beta_1} dy\, y^2 a(\beta_2 - y) + \frac{1}{\phi'_B r_B{}^2}\int_0^{\beta_3-\beta_2} dy\, y^2 a(\beta_2 + y)\right] + \frac{n}{\sigma_{out}a(\beta_4)}\left[\frac{1}{\phi'_A r_A{}^2}\int_0^{\beta_5-\beta_4} dy\, y^2 a(\beta_4 + y) + \frac{1}{\phi'_B r_B{}^2}\int_0^{\beta_4-\beta_3} dy\, y^2 a(\beta_4 - y)\right]\right) \quad (67)$$

Inserting the expressions for the surface coverage gives:

$$F_{str} = \frac{1}{\phi}\frac{\pi^2R^2}{8v(1)}\left(\frac{3}{\phi'_A r_A{}^2}\left[\int_0^{\beta_2-\beta_1} dy\, y^2 a(\beta_2 - y) + \int_0^{\beta_5-\beta_4} dy\, y^2 a(\beta_4 + y)\right] + \frac{3}{\phi'_B r_B{}^2}\left[\int_0^{\beta_4-\beta_3} dy\, y^2 a(\beta_4 - y) + \int_0^{\beta_3-\beta_2} dy\, y^2 a(\beta_2 + y)\right]\right) \quad (68)$$

which then can be written in terms of the stretching integrals defined in eqs 15−18 in the main text:

$$F_{str} = \frac{1}{\phi}\frac{\pi^2R^2}{8v(1)}\left(\frac{1}{\phi'_A r_A{}^2}[I'_A + I''_A] + \frac{1}{\phi'_B r_B{}^2}[I'_B + I''_B]\right) \quad (69)$$

## References and Notes

(1) Hajduk, D. A.; Kossuth, M. B.; Hillmyer, M. A.; Bates, F. S. *J. Phys. Chem. B* **1998**, *102*, 4269.
(2) Warriner, H. E.; Idziak, S. H. J.; Slack, N. L.; Davidson, P.; Safinaya, C. R. *Science* **1996**, *271*, 969.
(3) Won, Y.-Y.; Davis, H. T.; Bates, F. S. *Science* **1999**, *283*, 960.
(4) Yu, K.; Eisenberg, A. *Macromolecules* **1998**, *31*, 3509.
(5) Bates, F. S.; Fredrickson, G. H. *Annu. Rev. Phys. Chem.* **1990**, *41*, 525.
(6) Bang, J.; Jain, S.; Li, Z.; Lodge, T. P.; Pedersen, J. S.; Kesselman, E.; Talmon, Y. *Macromolecules* **2006**, *39*, 1199.
(7) Zupancich, J. A.; Bates, F. S.; Hillmyer, M. A. *Macromolecules* **2006**, *39*, 4286.
(8) Jain, S.; Bates, F. S. *Science* **2003**, *300*, 460.
(9) Khanna, K.; Chang, T. T.; Kindt, J. T. *J. Chem. Phys.* **2006**, *124*, 036102-1.
(10) Kindt, J. T. *J. Chem. Phys.* **2002**, *106*, 8223.
(11) Kindt, J. T.; Gelbart, W. M. *J. Chem. Phys.* **2001**, *114*, 1432.
(12) Haluska, C. K.; Gozdz, W. T.; Döbereiner, H. G.; Forster, S.; Gompper, G. *Phys. Rev. Lett.* **2002**, *89*, 238302−1.
(13) Döbereiner, H. G. *Curr. Opin. Colloid Interface Sci.* **2000**, *5*, 256.
(14) Cornelissen, J. J. L. M.; Fischer, M.; Sommerdijk, N. A. J. M.; Nolte, R. J. M. *Science* **1998**, *280*, 1427.

(15) Dischler, B. M.; Won, Y.-Y.; Ege, D. S.; Lee, J. C.-M.; Bates, F. S.; Discher, D.; Hammer, D. A. *Science* **1999**, *284*, 1143.
(16) Dischler, B. M.; Hammer, D. A.; Bates, F. S.; Discher, D. *Curr. Opin. Colloid Interface Sci.* **2000**, *5*, 125.
(17) Lee, J. C.-M.; Bermudez, H.; Dischler, B. M.; Sheehan, M. A.; Won, Y.-Y.; Bates, F. S.; Discher, D.; Hammer, D. A. *Biotechnol. Bioeng.* **2000**, *73*, 135.
(18) DeGennes, P. G. *Scaling Concepts in Polymer Physics*; Cornell University Press: Ithaca, NY, 1979.
(19) Zhang, L.; Barlow, R. J.; Eisenberg, A. *Macromolecules* **1995**, *28*, 6055.
(20) Zhulina, E. B.; Birshtein, T. M. *Polym. Sci. U.S.S.R.* **1985**, *27*, 570.
(21) Birshtein, T. M.; Zhulina, E. B. *Polymer* **1989**, *30*, 170.
(22) Halperin, A. *Macromolecules* **1987**, *20*, 29434.
(23) Izzo, D.; Marques, C. M. *Macromolecules* **1993**, *26*, 7189.
(24) Izzo, D.; Marques, C. M. *Macromolecules* **1997**, *30*, 6544.
(25) Zhulina, E. B.; Adam, M.; LaRue, I.; Sheiko, S. S.; Rubinstein, M. *Macromolecules* **2005**, *38*, 5330.
(26) Milner, S. T.; Witten, T. A.; Cates, M. E. *Macromolecules* **1988**, *21*, 2610.
(27) Milner, S. T.; Witten, T. A.; Cates, M. E. *Europhys. Lett.* **1988**, *5*, 413.
(28) Semenov, A. N. *JETP Lett.* **1985**, *88*, 1242.
(29) Zilman, A.; Tlusty, T.; Safran, S. A. *J. Chem. Phys.* **2003**, *15*, S57.
(30) Tlusty, T.; Safran, S.; Strey, R. *Phys. Rev. Lett.* **2000**, *84*, 1244.
(31) Larsen, A. L.; Terentjev, E. M. *Macromolecules* **2006**, *39*, 9497.
(32) Olmsted, P. D.; Milner, S. T. *Macromolecules* **1998**, *31*, 4011.
(33) Bates, F. S.; Fredrickson, G. H. *Macromolecules* **1994**, *27*, 1065.
(34) Bibette, J.; Morse, D. C.; Witten, T. A.; Weitz, D. A. *Phys. Rev. Lett.* **1992**, *69*, 2439.
(35) Olmsted, P. D. In *Soft Condensed Matter Physics in Molecular and Cell Biology*, 1st ed.; Taylor and Francis Group: Boca Raton, FL, 2006.
(36) Thomas, E. L.; Alward, D. B.; Kinning, D. J.; Martin, D. C.; Handlin, D. L.; Fetters, L. J. *Macromolecules* **1986**, *19*, 2197.
(37) Hasegawa, H.; Tanaka, H.; Yamasaki, K.; Hashimoto, T. *Macromolecules* **1987**, *20*, 1641.

MA061417D